

Ion Density Deviations in Polyelectrolyte Microcapsules: Influence on Biosensors

Qiyun Tang^a and Alan R. Denton^{*a}

Received 24th June 2014, Accepted 22nd August 2014

DOI: 10.1039/c4cp02773f

Polyelectrolyte microcapsules loaded with fluorescent dyes have been proposed as biosensors to monitor local pH and ionic strength for diagnostic purposes. In the case of charged microcapsules, however, the local electric field can cause deviations of ion densities inside the cavities, potentially resulting in misdiagnosis of some diseases. Using nonlinear Poisson-Boltzmann theory, we systematically investigate these deviations induced by charged microcapsules. Our results show that the microcapsule charge density, as well as the capsule and salt concentrations, contribute to deviations of local ion concentrations and pH. Our findings are relevant for applications of polyelectrolyte microcapsules with encapsulated ion-sensitive dyes as biosensors.

1 Introduction

Polyelectrolyte (PE) microcapsules, polymeric particles whose hollow cavities can be loaded with dye molecules¹, have attracted great attention in the past decade due to their potential biomedical applications², such as therapeutic drug delivery^{3,4} and diagnostics^{5–8}. Among the various experimental methods developed to fabricate microcapsules, one of the most attractive is layer-by-layer (LBL) assembly, due to its precise control of the capsule size, thickness, shape, and functions⁹. The LBL technique uses diverse driving forces, such as electrostatic interactions⁵, van der Waals interactions¹⁰, hydrogen bonding^{11,12}, guest-host interactions¹³, covalent bonding^{14,15}, and base-pair interactions¹⁶, to deposit the multi-layer films onto colloidal and nanoparticle templates, followed by the removal of sacrificial templates. When their cavities are loaded with therapeutic drugs, fluorescent dyes, or chemical reactants, such microcapsules can function as drug delivery vehicles^{4,17}, precise optical ratiometric biosensors^{18–22}, or bioreactors^{23,24}.

Recently, much interest has focused on applications of PE microcapsules loaded with ion-sensitive dyes as biosensors to monitor local ion concentrations, such as pH, in cellular environments^{5,21,25–34}. For example, Kreft *et al.*²¹ introduced PE microcapsules loaded with pH-sensitive SNARF-1 dye molecules to monitor the local pH within the alkaline cell medium and the acidic endosomal/lysosomal compartments. Recently, triple-labeled PE microcapsules loaded with two pH-sensitive dyes and one pH-insensitive dye, were also fabricated to measure the local pH in real time in living cells²⁹. Del Mercato *et al.*²⁸ demonstrated that double-wall barcoded sensor capsules can be used for multiplexed

detection of protons and sodium and potassium ions in parallel. These capsule-based sensor systems offer advantages in practical applications. First, the dye molecules are encapsulated in small cavities at high local concentrations, leading to high resolution optical images. Second, the dye molecules can be encapsulated in biocompatible PE microcapsules³⁵ to circumvent the toxicity in cellular environments and detect the local ion concentration in real time. Third, sensing and labeling dyes can be separately loaded in the cavities and walls of the microcapsules, providing a promising procedure for multiplexed sensing²⁸. These microcapsule-based chemical sensors have potential biomedical applications in the diagnosis of certain diseases^{5–8}.

In the LBL technique, microcapsules are often formed by exploiting electrostatic interactions to alternately adsorb PE layers onto oppositely charged templates. The PE shells, which become charged by dissociating counterions into aqueous solution, generate an electric field that influences the ion distributions (such as local pH) near the microcapsule shells. Previous work has shown that the ionic strength variations between bulk and charged surface regions may be significant^{36–39}. For example, Janata^{36,37} pointed out that bulk-surface interactions should be considered for the pH shift in optical sensors. Bostrom *et al.*³⁸ showed that ion-specific dispersion potentials near biological flat membranes could induce ion and pH gradients. Zhang *et al.*³⁹ experimentally demonstrated that surface charges can contribute significantly to local ion concentrations and sensor read-out. This phenomenon influences, in turn, the measured concentrations of ions in microcapsule cavities. Understanding these deviations is of great significance in biomedical applications, for example, to avoid misdiagnosis of diseases, such as early-stage cancer^{40–42}. Previous experiments^{43,44} and theoretical models^{43,45} have demonstrated that the pH inside microcapsules

^a Department of Physics, North Dakota State University, Fargo, ND 58108-6050, USA. E-mail: alan.denton@ndsu.edu

can differ from that outside. This difference was attributed mainly to semipermeability of the capsules, which impedes diffusion of one species of small ion across the capsule wall and generates Donnan equilibrium. To the best of our knowledge, however, there is still no theoretical work to quantitatively investigate the deviations in ion concentration induced by charged microcapsules.

The goal of this paper is to analyze the impact of the electric field of ionized PE shells on the performance of microcapsules as biosensors in aqueous solutions. By employing nonlinear Poisson-Boltzmann theory, we systematically calculate the deviation of ion density inside microcapsule cavities induced by charged shells. We find that the redistribution of ions inside the cavities of negatively charged capsules shifts the pH, as would be measured by encapsulated fluorescent dyes, towards lower (more acidic) values. The magnitude of the shift strongly depends on the charge density of the microcapsules, and on the capsule and salt concentrations. Our work differs from previous reports of pH deviations^{43–45} in that, in our model, the capsule wall is permeable to all ion species, and the predicted deviations of ion concentration and pH are not related to semipermeability of the capsules. Our results demonstrate that electric charge can influence the ability of ionic microcapsules to function as biosensors, which should stimulate experiments and simulations.

The remainder of the paper is organized as follows. In the next section, we describe our model and theoretical methods. In Sec. 3, we present results for the influence of charge density, and of capsule and salt concentrations, on the variation of ion distributions between the cavity and bulk regions. We then discuss advantages and limitations of our methods and prospects for future studies. Finally, in Sec. 4, we summarize and emphasize implications for practical applications.

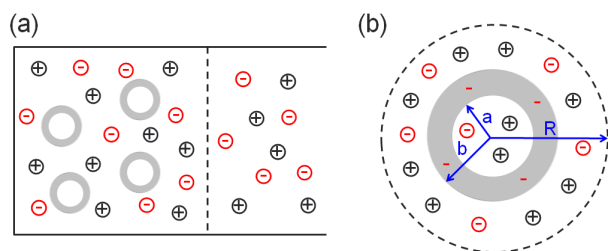


Fig. 1 (a) Primitive model: an aqueous solution of polyelectrolyte microcapsules (shaded rings) and positive and negative microions dispersed in a uniform dielectric (water). (b) Cell model: a single microcapsule, modeled as a uniformly charged shell (shaded ring) of valence Z and inner and outer radii a and b , centered in a spherical cell of radius R .

2 Models and Methods

We consider a solution of microcapsules, consisting of spherical shells of cross-linked PE chains. In a polar solvent (here water), the shells acquire charge through dissociation of counterions from the polymer backbones. The shells are permeable to water and small ions and enclose cavities that are filled with an aqueous solution, whose ionic strength can differ from that of the bulk solution. In Donnan equilibrium, the microcapsules are confined to a fixed volume, while the microions (counterions, salt ions) and solvent can freely exchange with a salt reservoir, e.g., via a semi-permeable membrane [Fig. 1(a)].

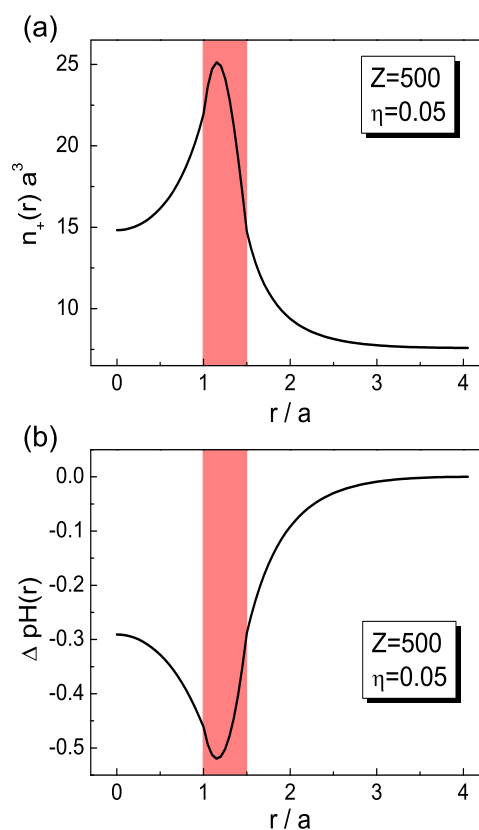


Fig. 2 (a) Reduced cation number density and (b) deviation of local pH from its bulk value (at cell edge) vs. radial distance from center of a PE microcapsule of inner shell radius $a = 50$ nm, outer radius $b = 75$ nm, valence $Z = 500$, and dielectric constant ratio $\chi = 0.5$, in an aqueous solution of microcapsule volume fraction $\eta = 0.05$ and reservoir salt concentration $n_0 = 0.1$ mM. Shaded bar indicates shell region.

We start from the primitive model⁴⁶, which reduces the solvent to a dielectric continuum of dielectric constant ϵ , and further idealize the dense network of PE chains and water

within a microcapsule shell as a uniform medium with dielectric constant ϵ_{shell} , fixed charge Ze , and uniform charge number density, $n_f(r) = Z/V_{\text{shell}}$ ($a < r < b$), confined to a volume $V_{\text{shell}} = (4\pi/3)(b^3 - a^3)$, between the inner radius a and outer radius b [Fig. 1(b)]. We assume that the water within the cavity ($r < a$) has a dielectric constant equal to that in bulk. In the PE shell, however, we assume $\epsilon_{\text{shell}} < \epsilon$, since PE microgels are known to have dielectric constants lower than that of bulk water^{47,48}. Finally, we model the microions simply as point charges. Although neglecting charge discreteness and ion-specific effects due to hydration, this coarse-grained model is constructed to capture the essential physical features of real PE microcapsules.

The substantial asymmetry in size and charge between polyions and microions motivates the cell model⁴⁹. For spherical polyions, such as microcapsules, the cell model represents a bulk solution by a spherical cell of radius R , centered on a single polyion. The cell contains a neutralizing number of counterions and coions in a volume determined by the polyion volume fraction $\eta = (b/R)^3$ [Fig. 1(b)]. For simplicity, we assume here monovalent microions, whose correlations with one another are sufficiently weak to justify a mean-field approach, in particular, a Poisson-Boltzmann theory.

The Poisson-Boltzmann (PB) theory of polyelectrolyte solutions combines the exact Poisson equation with the Boltzmann approximation for the ion density distribution^{46,49–51}. In the primitive model, in which the solvent has a uniform dielectric constant ϵ , the Poisson equation,

$$\nabla^2 \phi(\mathbf{r}) = -\frac{4\pi}{\epsilon} \rho(\mathbf{r}), \quad (1)$$

relates the electrostatic potential $\phi(\mathbf{r})$ at position \mathbf{r} to the local charge density, $\rho(\mathbf{r}) = e[n_+(\mathbf{r}) - n_-(\mathbf{r}) - n_f(\mathbf{r})]$, which includes the number densities of both mobile microions, $n_{\pm}(\mathbf{r})$, and fixed ions on the PE chains, $n_f(\mathbf{r})$. Equation (1) can also be expressed as

$$\nabla^2 \psi(\mathbf{r}) = -4\pi\lambda_B[n_+(\mathbf{r}) - n_-(\mathbf{r}) - n_f(\mathbf{r})] \quad (2)$$

by defining the reduced potential, $\psi \equiv e\phi/k_B T$, and the Bjerrum length, $\lambda_B \equiv e^2/\epsilon k_B T$, as the distance at which two elementary charges e interact with the typical thermal energy $k_B T$ at absolute temperature T . In Donnan equilibrium, the Boltzmann approximation for the microion number density distributions is

$$n_{\pm}(\mathbf{r}) = n_0 \exp[\mp \psi(\mathbf{r})], \quad (3)$$

where n_0 is the average number density of salt ion pairs in the reservoir. This mean-field approximation neglects short-range ion-ion correlations.

Combining the Poisson equation for the electrostatic potential [Eq. (2)] with the Boltzmann approximation for the microion density distributions [Eq. (3)] yields the PB equation,

$$\nabla^2 \psi(\mathbf{r}) = \kappa^2 \sinh \psi(\mathbf{r}) + 4\pi\lambda_B n_f(\mathbf{r}), \quad (4)$$

where $\kappa = \sqrt{8\pi\lambda_B n_0}$ is the screening constant in the salt reservoir. Implementation of the PB theory is facilitated by adopting the cell model, wherein solution of Eq. (4) is greatly eased by geometric symmetry and neglect of polyion-polyion correlations. In the spherical cell model, the PB equation simplifies to

$$\psi''(r) + \frac{2}{r}\psi'(r) = \begin{cases} \kappa^2 \sinh \psi(r), & 0 < r < a, \\ \frac{\kappa^2}{\chi} \sinh \psi(r) + \frac{3Z\lambda_B/\chi}{b^3 - a^3}, & a < r < b, \\ \kappa^2 \sinh \psi(r), & b < r < R, \end{cases} \quad (5)$$

where r is the radial distance from the center of the cell and $\chi = \epsilon_{\text{shell}}/\epsilon < 1$ is the ratio of the dielectric constant in the microcapsule shell to that in the bulk solvent.

The boundary conditions on Eq. (5) are clear. First, the electrostatic potential is continuous at the inner and outer boundaries of the microcapsule shell. Labelling the solutions in the three regions as $\psi_{\text{in}}(r)$ ($0 < r < a$), $\psi_{\text{shell}}(r)$ ($a < r < b$), and $\psi_{\text{out}}(r)$ ($b < r < R$), we have

$$\psi_{\text{in}}(a) = \psi_{\text{shell}}(a), \quad \psi_{\text{shell}}(b) = \psi_{\text{out}}(b). \quad (6)$$

Second, spherical symmetry requires that the electric field vanish at the center of the cell, while Gauss's law and electroneutrality require that the electric field vanish on the cell boundary:

$$\psi'_{\text{in}}(0) = 0, \quad \psi'_{\text{out}}(R) = 0. \quad (7)$$

Finally, continuity of the electric displacement on the inner and outer shell boundaries requires

$$\psi'_{\text{in}}(a) = \chi \psi'_{\text{shell}}(a), \quad \chi \psi'_{\text{shell}}(b) = \psi'_{\text{out}}(b). \quad (8)$$

We calculate the equilibrium microion distributions within the spherical cell by numerically solving the PB equation [Eq. (5)], along with the boundary conditions [Eqs. (6)-(8)], in the three radial regions (inside the cavity, in the shell, and outside the capsule), matching the solutions at the inner and outer shell boundaries using a two-dimensional root-finding algorithm⁵².

As an illustration of our method, Fig. 2(a) shows the cation number density in the vicinity of a negatively charged PE microcapsule of inner shell radius $a = 50$ nm, outer shell radius $b = 75$ nm, and valence $Z = 500$. The PE microcapsules are dispersed in room-temperature water ($\lambda_B = 0.72$ nm), with reservoir salt concentration $n_0 = 0.1$ mM, at a volume fraction $\eta = 0.05$ – corresponding to a cell radius $R = \eta^{-1/3}b \simeq 4.07a$. At such dilution, the microcapsules are sufficiently separated that the ion distributions within different cavities are essentially independent. The dielectric constant ratio is set as $\chi = 0.5$, which is consistent with hydrated PNIPAM microgels, whose dielectric constant ranges from 63 at 15°C to 17

at 40°C^{47,48}. Figure 2(a) demonstrates that the ion density inside the capsule exceeds the bulk value (at the cell boundary), confirming that the charged shell indeed redistributes the ion density near the microcapsule. Note the discontinuous slopes in Fig. 2 at the shell boundaries ($r = a, b$), which simply reflect the jump in dielectric constant between the shell and water.

Many recent experiments have focused on measurements of local pH using fluorescent dyes encapsulated in PE microcapsules. Within our theoretical framework, the local pH inside the PB cell is normally determined via $\text{pH}(r) = -\log([H^+](r))$, where $[H^+](r)$ denotes the hydronium ion concentration (in M) at radial distance r from the cell center. The local deviation of pH from its bulk value is then obtained via $\Delta\text{pH}(r) = -\log([H^+](r)/[H^+]_{\text{bulk}})$, where $[H^+]_{\text{bulk}}$ is the bulk hydronium concentration. In an alkaline environment, the pH can be defined, alternatively, from the concentration of hydroxide (OH^-) ions, giving rise to the deviation $\Delta\text{pH}(r) = \log([OH^-](r)/[OH^-]_{\text{bulk}})$.

Because the mean-field PB theory ignores ion-specific effects, it cannot distinguish hydronium ions from other monovalent cations, such as Na^+ or K^+ . Nevertheless, in the presence of an inhomogeneous electric field generated here by a charged microcapsule shell, the local deviation of hydronium concentration from its bulk value should be proportional to the local deviation of the concentration of all monovalent cations. Thus, we approximate the local deviation of pH from its bulk value by

$$\Delta\text{pH}(r) \simeq \begin{cases} -\log[n_+(r)/n_+(R)] & \text{(acidic)} \\ \log[n_-(r)/n_-(R)] & \text{(alkaline)} \end{cases} \quad (9)$$

where $n_+(R)$ and $n_-(R)$ are the cell model approximations for the bulk cation and anion densities, respectively. In the Boltzmann approximation [Eq. (3)], pH deviation is proportional to the electrostatic potential deviation:

$$\Delta\text{pH}(r) = (\log e)[\psi(r) - \psi(R)], \quad (10)$$

illustrating the direct connection between pH deviation and the electrostatic influence of the microcapsule, and providing a practical formula for calculations. Figure 2(b) shows the deviation of local pH based on the cation distribution in Fig. 2(a). For the chosen parameters, the local pH inside the negatively charged shell is lower than the bulk value within a range from 0.3 to 0.5. Also of experimental relevance is the average pH deviation, defined as an average over the volume of the cavity:

$$\langle\Delta\text{pH}\rangle \equiv \frac{3}{a^3} \int_0^a dr r^2 \Delta\text{pH}(r). \quad (11)$$

In the next section, we explore the dependence of ion distributions and pH deviation on the valence, size, and concentration of negatively charged microcapsules.

3 Results and Discussion

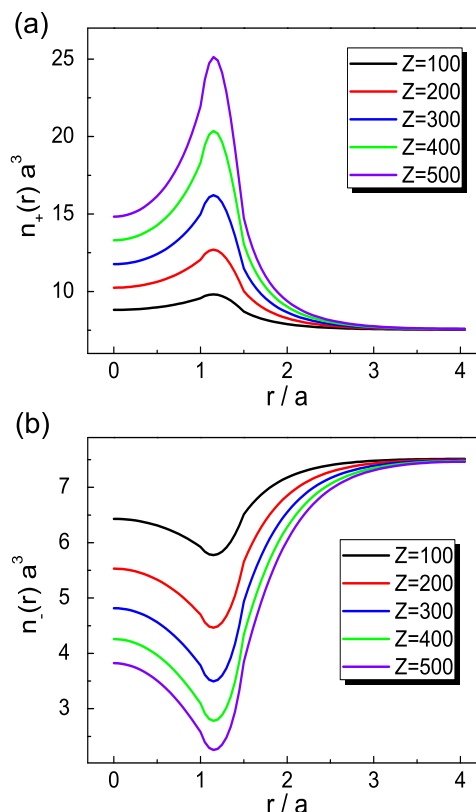


Fig. 3 Number densities of (a) cations and (b) anions inside cell for microcapsule valences $Z = 100, 200, 300, 400$, and 500 [bottom to top in (a), top to bottom in (b)]. (Other parameters are as in Fig. 2.)

3.1 Influence of Charge Density on pH Deviations inside Microcapsule Cavities

In this section, we systematically investigate the influence of a negatively charged microcapsule on ion density distributions within the PB cell model. In experiments, the microcapsule valence can be tuned by varying the shell composition, as well as bulk solution conditions (pH and salt concentration), and even temperature. Figure 3 shows the dependence of the ion distributions on the microcapsule valence, demonstrating that the cation density is higher than the bulk value throughout the cell, reaches a maximum within the shell, and increases with valence, from $Z = 100$ to $Z = 500$. Furthermore, with increasing microcapsule valence, the maximum increases, while the bulk cation density remains nearly constant, implying that the deviations of cation density induced by the charged shell are strongly determined by the capsule valence. Conversely, the

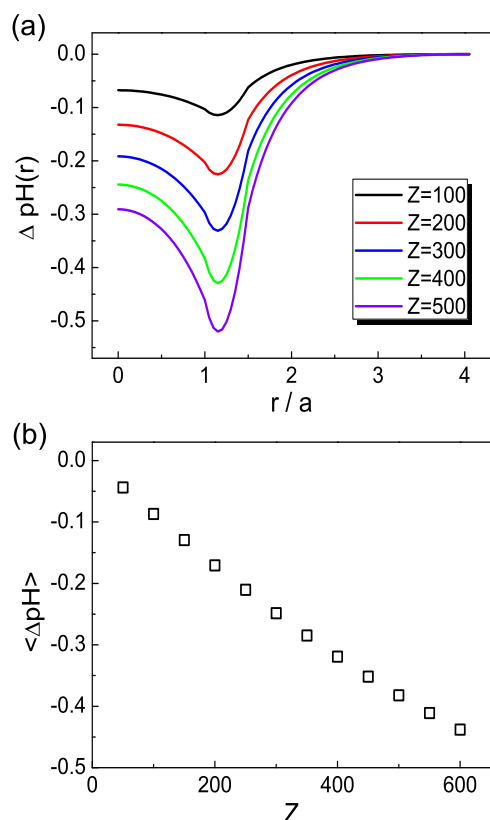


Fig. 4 (a) Deviation of local pH from its bulk value vs. radial distance from microcapsule center for valences $Z = 100, 200, 300, 400$, and 500 (top to bottom). (b) Average pH deviation inside cavity vs. valence. (See Fig. 2 for other parameters.)

anion density is lower than the bulk value, reaches a minimum within the shell, and decreases steadily with increasing valence. These deviations result from the attraction of cations (repulsion of anions) by the negatively charged shell.

In an acidic environment, the cation distribution induced by the charged capsule correlates with the deviation of pH from its bulk value, according to Eq. (9). As an example, Fig. 4 shows the distributions of local and average pH deviations over a range of microcapsule valences. With increasing valence, the pH inside the microcapsules falls increasingly below the bulk pH value, while the average pH deviation inside the capsule cavities increases in magnitude. At the highest valence considered here, the pH deviation from its bulk value in the cavity can approach -0.5 . A shift of this magnitude may be significant for proposed applications of PE microcapsules as pH sensors²¹, where encapsulated dye molecules fluoresce at frequencies that depend on the local pH. In an alkaline environment, essentially the same pH deviation is obtained from Eq. (9) when calculated using the anion density

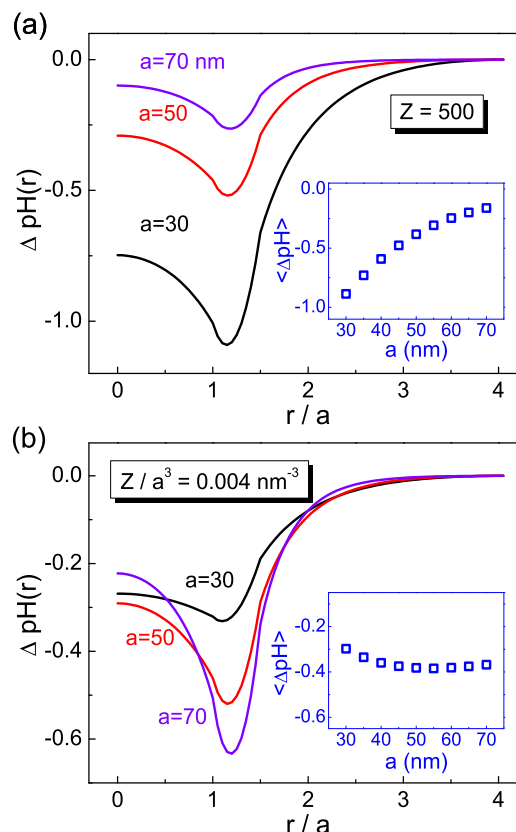


Fig. 5 Deviation of local pH vs. radial distance from microcapsule center for cavity inner radius $a = 30, 50, 70$ nm (outer radius $b = 1.5a = 45, 75, 105$ nm) at (a) fixed capsule valence $Z = 500$ and (b) fixed charge density $Z/a^3 = 0.004 \text{ nm}^{-3}$. Insets show variation of average pH deviation inside cavity with cavity radius. (Other parameters are as in Fig. 2.)

distribution. It is important to remember, however, that the valence of a PE microcapsule in solution may itself depend self-consistently on the local pH, since local pH can affect dissociation-association equilibrium and thus the degree of ionization of the PE chains making up the shell.

Next, we investigate the influence of microcapsule size on induced pH deviations. Although many recent experiments involve capsules that are a few microns in size^{21,28,29}, here we consider considerably smaller capsules, tens of nanometers in radius, which is the current limit of our numerical methods. As shown in Fig. 5(a), for fixed valence, as the cavity inner radius increases, the local and average pH deviations decrease in magnitude. This trend is to be expected, since for the same charge, the electric field inside of a larger capsule is weaker, resulting in less redistribution of ions. However, if the capsule size and valence vary together, at fixed valence density, the pH deviation is relatively insensitive to the capsule size (see

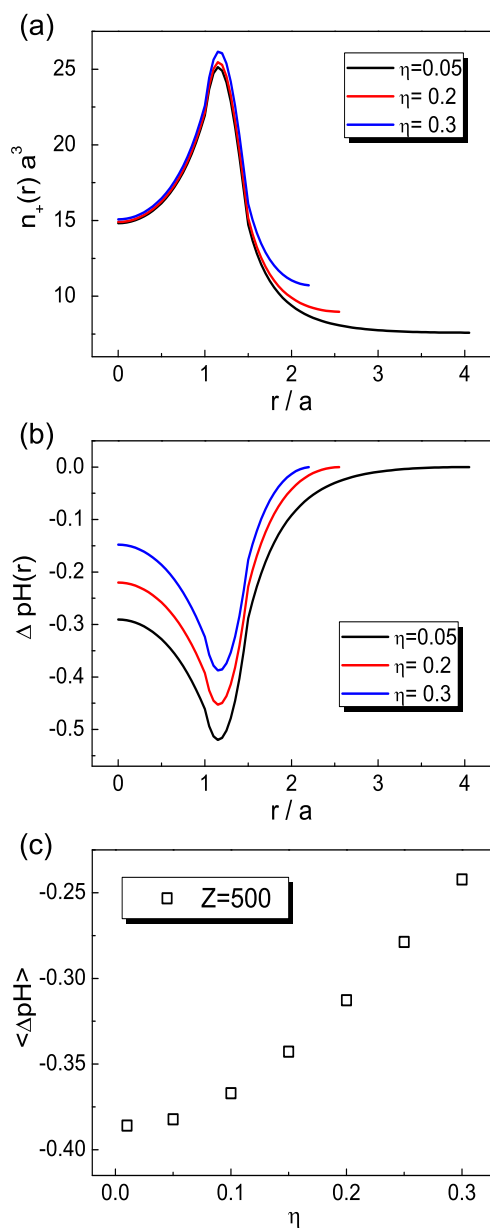


Fig. 6 (a) Cation number density and (b) local pH deviation for microcapsules of valence $Z = 500$ and volume fraction $\eta = 0.05, 0.2$, and 0.3 (bottom to top). (c) Average pH deviation in cavity vs. η . (See Fig. 2 for other parameters.)

Fig. 5(b)). It is worth noting that the pH deviations exhibited in Fig. 4 also reflect the dependence on charge density (with fixed capsule size). In experiments, charge densities are determined by both the density of the PE network and the degree of PE dissociation in solution. Extrapolation to larger capsules suggests that pH deviations inside the cavities of strongly

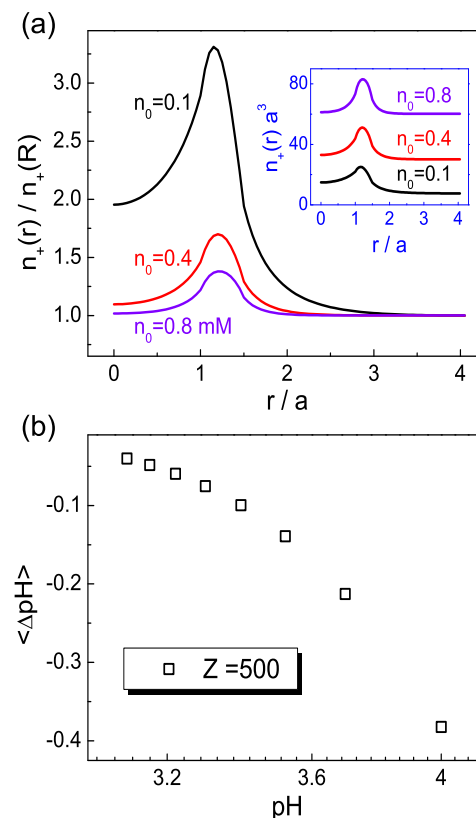


Fig. 7 (a) Local cation density, as a fraction of bulk density, at reservoir salt concentration $n_0 = 0.1, 0.4$, and 0.8 mM. Inset shows the corresponding cation number densities. (b) Average pH deviation vs. pH at $Z = 500$ and $a = 50$ nm. (See Fig. 2 for other parameters.)

dissociated PE capsules of the size studied in recent experiments^{21,28,29} may be significant.

From the above considerations, we conclude that charge density of PE shells is a major determiner of deviations of ion density and pH induced by charged microcapsules. Next, we show that even when the charge density remains constant, other factors can still influence ion concentrations inside of charged microcapsules.

3.2 Influence of Microcapsule and Salt Concentrations on pH Deviations

Among other factors that can affect ion density and pH deviations in microcapsule cavities, the first that we consider is the microcapsule volume fraction η , whose influence is illustrated in Fig. 6. For fixed shell charge density ($Z = 500, a = 50$ nm), Fig. 6(a) shows that the cation density inside the cavity remains essentially unchanged with increasing η (i.e., decreasing cell radius R), while outside the microcapsule, the bulk

cation concentration $n_+(R)$ steadily increases. Correspondingly, the pH deviation inside the cavity decreases with increasing η [Figs. 6(b) and 6(c)]. It follows that an inhomogeneous distribution of PE microcapsules can yield a spatial variation of pH deviation and that, in concentrated solutions, pH values measured from fluorescence of encapsulated dye molecules should be adjusted for concentration dependence.

Another factor that can affect deviations of ion densities in capsule cavities from their bulk values is the reservoir salt concentration n_0 . As illustrated in Fig. 7, for fixed capsule charge density ($Z = 500$, $a = 50$ nm), the deviation of cation density (and, therefore, pH) diminishes with increasing salt concentration. In the extreme case of a solution that contains predominantly H^+ cations, the reservoir salt concentration n_0 is directly related to the reservoir pH value via $pH = -\log n_0$. For such a deionized system, Fig. 7(b) shows that the average pH deviation inside the cavity induced by the charged shell is then strongly dependent on the bulk pH. This dependence indicates that the local pH measured by capsule-based sensors in low-pH acidic environments can deviate less than in acidic environments with higher pH. Therefore, in practical applications, the calibration of measured local pH to the actual values in cellular environments should also take into account the gradient of the pH deviation induced by the absolute local pH.

It should be mentioned that ion concentrations may depend also on temperature. This dependence is somewhat complicated, however, by the sensitivity of counterion dissociation and Donnan equilibrium to thermal fluctuations. Therefore, in this work, we simply assume fixed (room) temperature.

3.3 Discussion

We have demonstrated here that negatively charged PE microcapsules redistribute ion concentrations, resulting in accumulations of H^+ ions in their cavities and corresponding shifts of local pH to values lower than in bulk. The magnitude of the pH shift depends strongly on the microcapsule charge density, as well as on the capsule and salt ion concentrations. These results confirm that the ion concentrations measured by dye molecules encapsulated in charged PE microcapsule cavities can deviate from their bulk values, potentially leading to misdiagnosis of diseases^{40–42}. In this section, we discuss some limitations of Poisson-Boltzmann theory and several open questions for further investigation.

First, the PB theory implemented here cannot distinguish distinct monovalent ions. In this paper, we assume that density deviations induced by charged PE microcapsules are the same for all monovalent cations and choose H^+ as an example to illustrate the deviation of pH in the cavities of charged microcapsules. Our results can be easily extended to the detection of other monovalent ions, such as Na^+ and K^+ . Previous studies have shown, however, that ionic strength can influence

the local pH obtained from optical pH sensors^{36,37,53}. Thus, it is still not clear how specific interactions between different monovalent cations may influence deviations of ion concentrations and pH induced by charged microcapsules. Experiments and further modeling are required to address this issue.

A second issue deserving further discussion is the magnitude of the local pH deviation induced by negatively charged microcapsules. For the parameters considered in this paper, the pH shift is typically within the range 0.1 to 0.6. Although higher shell charge densities can induce shifts exceeding 1.0, the energy barrier across the shell in this case is larger than $2 k_B T$, which kinetically impedes ions from penetrating the capsule by thermal diffusion. The typical deviation magnitude of 0.5 observed in this paper is within the error bar of some recent experiments²⁹, implying that the measured pH deviations might be negligible. It is important to note, however, that the next generation of capsule-based biosensors will rely on higher spatial resolution of ion densities for practical applications, such as the diagnosis of cancer⁴⁰, and that the magnitude of pH deviations predicted by our modeling may become correspondingly significant.

The third issue on which we wish to elaborate is the microcapsule size. In this report, the outer shell radius is within the range 45–105 nm (see Fig. 5), due to limitations of our numerical methods. In most recent experiments, however, the microcapsules are a few microns in size^{21,28,29}. As we have demonstrated (Fig. 5), the deviation of ion density induced by a charged microcapsule remains nearly constant upon varying the capsule size at fixed charge density. In aqueous solutions, the charge of a microcapsule is determined mainly by the degree of PE dissociation. Most recent experiments, however, synthesized PE microcapsules via the LBL technique, alternately adsorbing PEs onto oppositely charged templates. For such complex architectures, it is still unknown how sensitive the degree of dissociation and charge density may be to varying microcapsule size. Further experiments and simulations are required to quantitatively relate the charge density and size of LBL-generated PE microcapsules.

Fourth, the PB theory is applicable only under conditions for which the microions are sufficient in number to be modeled as continuous fields. Moreover, the mean-field approximation, which neglects ion correlations, limits applications of the Poisson-Boltzmann theory to solutions containing only monovalent microions, such as H^+ , Na^+ , and K^+ . For multivalent ions such as Ca^{2+} ⁵⁴, Mg^{2+} ⁵⁵, Zn^{2+} ⁵⁶, and Fe^{3+} ⁵⁷, the deviations induced by charged PE microcapsules may be more complex, due to interionic correlations. Further simulations and more sophisticated theories that account for ion discreteness and correlations among multivalent ions are required to address these issues.

Finally, we emphasize the great practical importance of microcapsule-based biosensors, which provide powerful tools

for detection of ions in small volumes and diagnosis of cancer and other diseases^{40–42}. In aqueous solutions, charged microcapsules are known to redistribute neighboring ions, inducing deviations of ion densities and local pH. The results of our theoretical modeling verify the significance of these deviations, which will become increasingly significant with advances in spatial resolution of next-generation biosensors, and can guide and facilitate further explorations.

4 Conclusions

In summary, by implementing the nonlinear Poisson-Boltzmann theory in a cell model, we have theoretically demonstrated that charged polyelectrolyte microcapsules can induce deviations of ion concentrations inside their cavities. Our results show that the capsule charge density and the capsule and salt concentrations contribute to deviations of ion densities, such as pH, from their bulk values. Our findings are especially relevant for the design of microcapsules that encapsulate fluorescent dyes to serve as ionic biosensors for diagnostic purposes. The theoretical framework developed here can be easily extended to further investigate ionic strength deviations induced by charged semipermeable microcapsules.

Acknowledgments

This work was supported by the National Science Foundation under Grant No. DMR-1106331. We thank Andrew B. Croll and Damith Rozairo for discussions.

References

- 1 S. M. Borisov, T. Mayr, G. Mistlberger and I. Klimant, *Advanced Fluorescence Reporters in Chemistry and Biology II: Molecular Constructions, Polymers and Nanoparticles*, 2010, vol. 09, pp. 193–228.
- 2 L. L. del Mercato, P. Rivera-Gil, A. Z. Abbasi, M. Ochs, C. Ganas, I. Zins, C. Soennichsen and W. J. Parak, *Soft Matter*, 2010, **2**, 458–467.
- 3 S. De Koker, R. Hoogenboom and B. G. De Geest, *Chem. Soc. Rev.*, 2012, **41**, 2867–2884.
- 4 S. De Koker, L. J. De Cock, P. Rivera-Gil, W. J. Parak, R. A. Velty, C. Vervaet, J. P. Remon, J. Grooten and B. G. De Geest, *Adv. Drug Delivery Rev.*, 2011, **63**, 748–761.
- 5 B. G. De Geest, S. De Koker, G. B. Sukhorukov, O. Kreft, W. J. Parak, A. G. Skirtach, J. Demeester, S. C. De Smedt and W. E. Hennink, *Soft Matter*, 2009, **5**, 282–291.
- 6 W. Tong, X. Song and C. Gao, *Chem. Soc. Rev.*, 2012, **41**, 6103–6124.
- 7 M. Adamczak, H. J. Hoel, G. Gaudernack, J. Barbasz, K. Szczepanowicz and P. Warszynski, *Colloid Surf. B-Biointerfaces*, 2012, **90**, 211–216.
- 8 J. Peteiro-Cattelle, M. Rodriguez-Pedreira, F. Zhang, P. Rivera Gil, L. L. del Mercato and W. J. Parak, *Nanomedicine*, 2009, **4**, 967–979.
- 9 F. Caruso, R. A. Caruso and H. Möhwald, *Science*, 1998, **282**, 1111–1114.
- 10 T. Kida, M. Mouri and M. Akashi, *Angew. Chem. Int. Ed.*, 2006, **45**, 7534–7536.
- 11 G. K. Such, A. P. R. Johnston and F. Caruso, *Chem. Soc. Rev.*, 2011, **40**, 19–29.
- 12 E. Kharlampieva and S. A. Sukhishvili, *Polym. Rev.*, 2006, **46**, 377–395.
- 13 Z. Wang, Z. Feng and C. Gao, *Chem. Mater.*, 2008, **20**, 4194–4199.
- 14 Y. J. Zhang, S. G. Yang, Y. Guan, W. X. Cao and J. Xu, *Macromolecules*, 2003, **36**, 4238–4240.
- 15 L. Duan, Q. He, X. Yan, Y. Cui, K. Wang and J. Li, *Biochem. Biophys. Res. Commun.*, 2007, **354**, 357–362.
- 16 A. P. R. Johnston, E. S. Read and F. Caruso, *Nano Lett.*, 2005, **5**, 953–956.
- 17 P. Rivera-Gil, S. De Koker, B. G. De Geest and W. J. Parak, *Nano Lett.*, 2009, **9**, 4398–4402.
- 18 L. Shen, X. Lu, H. Tian and W. Zhu, *Macromol.*, 2011, **44**, 5612–5618.
- 19 U. Reibetanz, M. H. A. Chen, S. Mutukumaraswamy, Z. Y. Liaw, B. H. L. Oh, E. Donath and B. Neu, *J. Biomater. Sci.*, 2011, **22**, 1845–1859.
- 20 L. I. Kazakova, L. I. Shabarchina and G. B. Sukhorukov, *Phys. Chem. Chem. Phys.*, 2011, **13**, 11110–11117.
- 21 O. Kreft, A. M. Javier, G. B. Sukhorukov and W. J. Parak, *J. Mater. Chem.*, 2007, **17**, 4471–4476.
- 22 M. McShane and D. Ritter, *J. Mater. Chem.*, 2010, **20**, 8189–8193.
- 23 B. Staedler, A. D. Price, R. Chandrawati, L. Hosta-Rigau, A. N. Zelikin and F. Caruso, *Nanoscale*, 2009, **1**, 68–73.
- 24 D. G. Shchukin and G. B. Sukhorukov, *Adv. Mater.*, 2004, **16**, 671–682.
- 25 E. Kuwana, F. Liang and E. M. Sevick-Muraca, *Biotechnol. Prog.*, 2004, **20**, 1561–1566.
- 26 U. Reibetanz, M. H. A. Chen, S. Mutukumaraswamy, Z. Y. Liaw, B. H. L. Oh, S. Venkatraman, E. Donath and B. Neu, *Biomacromolecules*, 2010, **11**, 1779–1784.
- 27 L. L. del Mercato, A. Z. Abbasi and W. J. Parak, *Small*, 2011, **7**, 351–363.
- 28 L. L. del Mercato, A. Z. Abbasi, M. Ochs and W. J. Parak, *ACS Nano*, 2011, **5**, 9668–9674.
- 29 X. Song, H. Li, W. Tong and C. Gao, *J. Colloid Interface Sci.*, 2014, **416**, 252–257.
- 30 L. I. Kazakova, L. I. Shabarchina, S. Anastasova, A. M.

- Pavlov, P. Vadgama, A. G. Skirtach and G. B. Sukhorukov, *Anal. Bioanal. Chem.*, 2013, **405**, 1559–1568.
- 31 H. Sun, R. V. Benjaminsen, K. Almdal and T. L. Andresen, *Bioconjugate Chem.*, 2012, **23**, 2247–2255.
- 32 D. Jimenez de Aberasturi, J.-M. Montenegro, I. Ruiz de Larramendi, T. Rojo, T. A. Klar, R. Alvarez-Puebla, L. M. Liz-Marzan and W. J. Parak, *Chem. Mater.*, 2012, **24**, 738–745.
- 33 P. Rivera-Gil, M. Nazarenus, S. Ashraf and W. J. Parak, *Small*, 2012, **8**, 943–948.
- 34 H.-Y. Lee, K. R. Tiwari and S. R. Raghavan, *Soft Matter*, 2011, **7**, 3273–3276.
- 35 A. R. Patel, C. Remijn, A.-i. M. Cabero, P. C. M. Heussen, J. W. M. S. ten Hoorn and K. P. Velikov, *Adv. Funct. Mater.*, 2013, **23**, 4710–4718.
- 36 J. Janata, *Anal. Chem.*, 1987, **59**, 1351–1356.
- 37 J. Janata, *Anal. Chem.*, 1992, **64**, 921A–927A.
- 38 M. Bostrom, D. R. M. Williams and B. W. Ninham, *Langmuir*, 2002, **18**, 8609–8615.
- 39 F. Zhang, Z. Ali, F. Amin, A. Feltz, M. Oheim and W. J. Parak, *Chem. Phys. Chem.*, 2010, **11**, 730–735.
- 40 R. Weissleder, *Science*, 2006, **312**, 1168–1171.
- 41 P. Rivera Gil and W. J. Parak, *ACS Nano*, 2008, **2**, 2200–2205.
- 42 J. Xie, G. Liu, H. S. Eden, H. Ai and X. Chen, *Acc. Chem. Res.*, 2011, **44**, 883–892.
- 43 G. B. Sukhorukov, M. Brumen, E. Donath and H. Möhwald, *J. Phys. Chem. B*, 1999, **103**, 6434–6440.
- 44 D. Haložan, C. Déjugnat, M. Brumen and G. B. Sukhorukov, *J. Chem. Inf. Model.*, 2005, **45**, 1589–1592.
- 45 D. Haložan, G. B. Sukhorukov, M. Brumen, E. Donath and H. Möhwald, *Acta Chim. Slov.*, 2007, **54**, 598–604.
- 46 R. A. Marcus, *J. Chem. Phys.*, 1955, **23**, 1057–1068.
- 47 M. Parthasarathy and D. J. Klingenberg, *Mater. Sci. Eng.*, 1996, **17**, 57–103.
- 48 P. S. Mohanty, A. Yethiraj and P. Schurtenberger, *Soft Matter*, 2012, **8**, 10819–10822.
- 49 H. Wennerström, B. Jönsson and P. Linse, *J. Chem. Phys.*, 1982, **76**, 4665–4670.
- 50 A. R. Denton, *Phys. Rev. E*, 2003, **67**, 011804–1–10.
- 51 A. R. Denton, *J. Phys.: Condens. Matter*, 2010, **22**, 364108–1–8.
- 52 W. H. Press, S. A. Teukolsky, W. T. Vetterling and B. P. Flannery, *Numerical Recipes: The Art of Scientific Computing*, Cambridge University Press, New York, 3rd edn, 2007.
- 53 B. M. Weidgans, C. Krause, I. Klimant and O. S. Wolfbeis, *Analyst*, 2004, **129**, 645–650.
- 54 H. A. Clark, R. Kopelman, R. Tjalkens and M. A. Philbert, *Anal. Chem.*, 1999, **71**, 4837–4843.
- 55 E. J. Park, M. Brasuel, C. Behrend, M. A. Philbert and R. Kopelman, *Anal. Chem.*, 2003, **75**, 3784–3791.
- 56 J. P. Sumner, J. W. Aylott, E. Monson and R. Kopelman, *Analyst*, 2002, **127**, 11–16.
- 57 J. P. Sumner and R. Kopelman, *Analyst*, 2005, **130**, 528–533.